

1 *Short article*

2 **High-resolution glucose fate-mapping reveals *LDHB*-dependent lactate  
3 production by human pancreatic  $\beta$  cells**

4 Federica Cuozzo<sup>1</sup>, Daniela Nasteska<sup>1</sup>, Zicong Jiao<sup>1</sup>, Hannah R. Smith<sup>1</sup>, Caroline Bonner<sup>2</sup>,  
5 Julie Kerr-Conte<sup>2</sup>, Francois Pattou<sup>2</sup>, Rita Nano<sup>3,4</sup>, Lorenzo Piemonti<sup>3,4</sup>, Jennie Roberts<sup>1</sup>,  
6 Gareth G. Lavery<sup>1,5</sup>, Ildem Akerman<sup>1</sup>, Daniel A. Tennant<sup>1\*</sup>, Christian Ludwig<sup>1\*</sup> and David J.  
7 Hodson<sup>1,6\*</sup>

8  
9 <sup>1</sup>Institute of Metabolism and Systems Research (IMSR), and Centre of Membrane Proteins  
10 and Receptors (COMPARE), University of Birmingham, Birmingham, UK.

11 <sup>2</sup>University of Lille, Institut National de la Santé et de la Recherche Médicale (INSERM),  
12 Centre Hospitalier Universitaire de Lille (CHU Lille), Institute Pasteur Lille, U1190 -European  
13 Genomic Institute for Diabetes (EGID), F59000, Lille, France.

14 <sup>3</sup>San Raffaele Diabetes Research Institute, IRCCS Ospedale San Raffaele, Milan, Italy.

15 <sup>4</sup>Vita-Salute San Raffaele University, Milan, Italy.

16 <sup>5</sup>Centre for Health, Ageing and Understanding Disease, Department of Biosciences, School  
17 of Science and Technology, Nottingham Trent University, Nottingham, UK.

18 <sup>6</sup>Oxford Centre for Diabetes, Endocrinology and Metabolism (OCDEM), NIHR Oxford  
19 Biomedical Research Centre, Churchill Hospital, Radcliffe Department of Medicine, University  
20 of Oxford, Oxford, UK.

21

22

23 \*Correspondence should be addressed to:

24 [d.hodson@ocdem.ox.ac.uk](mailto:d.hodson@ocdem.ox.ac.uk), [c.ludwig@bham.ac.uk](mailto:c.ludwig@bham.ac.uk), [d.tennant@bham.ac.uk](mailto:d.tennant@bham.ac.uk)

25

26

27 **Key words:** Glucose tracing, islet, metabolism, pyruvate, lactate, LDH, pyruvate  
28 dehydrogenase, GC-MS, NMR

29

30

31 **ABSTRACT**

32 Using  $^{13}\text{C}_6$  glucose labeling coupled to GC-MS and 2D  $^1\text{H}$ - $^{13}\text{C}$  HSQC NMR spectroscopy, we  
33 have obtained a comparative high-resolution map of glucose fate underpinning steady state  
34 insulin release and  $\beta$  cell function. In both mouse and human islets, the contribution of glucose  
35 to the TCA cycle is similar. Pyruvate-fueling of the TCA cycle is found to be mediated primarily  
36 by the activity of pyruvate dehydrogenase (PDH), with only a limited contribution from pyruvate  
37 carboxylase (PC). While conversion of pyruvate to lactate by lactate dehydrogenase (LDH)  
38 can be detected in both species, lactate accumulation via this route is six-fold higher in human  
39 islets. Transcriptomic analysis reveals that human  $\beta$  cells specifically express lactate  
40 dehydrogenase B (LDHB) at high levels, in keeping with the phenotype of patients harboring  
41 gain-of-function mutations in MCT1/ SLC16A1 (HHF7). Thus, glycolytically-derived acetyl CoA  
42 preferentially feeds the TCA cycle in both mouse and human  $\beta$  cells. However, human  $\beta$  cells  
43 possess the machinery needed to generate extra-mitochondrial lactate, which might reflect a  
44 key mechanism to balance the reducing activity of NADH-producing pathways.

45

## 46 INTRODUCTION

47  $\beta$  cells are highly-adapted as glucose sensors and need to balance glucose-dependent insulin  
48 release with housekeeping metabolic functions. The traditional view of  $\beta$  cell metabolism  
49 focuses on a tight relationship between blood glucose concentration, oxidative  
50 phosphorylation and stimulus-secretion coupling. Following a rise in glycemia, glucose enters  
51 the  $\beta$  cell through facilitated transport via low affinity glucose transporters (GLUT1 and GLUT2  
52 in humans and rodents, respectively) (De Vos et al., 1995; Thorens et al., 1988). Glucose is  
53 then phosphorylated by a low affinity hexokinase, glucokinase (GK), leading to closure of the  
54 ATP-sensitive potassium ( $K_{ATP}$ ) channels (reviewed in (Rorsman and Ashcroft, 2018; Rutter  
55 et al., 2015)). The increase in membrane voltage then drives  $Ca^{2+}$  flux through voltage-  
56 dependent  $Ca^{2+}$  channels (Rorsman and Ashcroft, 2018), which together with amplifying  
57 signals (amino acids, isocitrate, cAMP etc) (Ferdaoussi et al., 2015; Henquin, 2000; Rutter et  
58 al., 2015), drives first and second phase insulin granule exocytosis. Direct conversion of  
59 pyruvate to lactate is thought to be suppressed in the  $\beta$  cell due to low levels of lactate  
60 dehydrogenase A (LDHA) (Ainscow et al., 2000; Pullen et al., 2010; Schuit et al., 2012; Sekine  
61 et al., 1994), ensuring that the majority of pyruvate enters the TCA cycle.

62 Recent studies have challenged the canonical view of  $\beta$  cell metabolism by showing that  
63 ATP/ADP generation is highly compartmentalized, with the extra-mitochondrial  
64 phosphoenolpyruvate (PEP) cycle being a major trigger of  $K_{ATP}$  channel closure and insulin  
65 secretion (Foster et al., 2022; Lewandowski et al., 2020). Following membrane depolarization  
66 and  $Ca^{2+}$  influx, the rise in ADP activates oxidative phosphorylation (OxPhos) to sustain insulin  
67 secretion. These two complementary states are believed to dictate the mitochondrial fate of  
68 pyruvate. The electrically silent phase, which is characterized by a high ATP/ADP ratio, raises  
69 mitochondrial voltage to stall the TCA cycle, and activate anaplerotic flux through pyruvate  
70 carboxylase (PC) and the PEP cycle to support pyruvate kinase (PK) and initiate insulin  
71 secretion. Following membrane depolarization, the rise in ADP supports a highly oxidative  
72 state that depends on high TCA cycle flux and pyruvate consumption by pyruvate  
73 dehydrogenase (PDH), which supports OxPhos and sustained secretion (Foster et al., 2022;  
74 Lewandowski et al., 2020; Merrins et al., 2022).

75 Despite the clear importance of metabolism for  $\beta$  cell insulin release and phenotype, we are  
76 still lacking a high-resolution, integrated view of  $\beta$  cell glucose fate. In particular, most data  
77 using glucose tracing and GC-MS/NMR spectroscopy has been derived from insulinoma cell  
78 lines, which provide the requisite cell mass for metabolite detection/annotation. However,  
79 insulinoma cell lines have to balance the need for insulin secretion with proliferation, an  
80 energy-consuming process (Alves et al., 2015; Cline et al., 2004; Cline et al., 2011; Lu et al.,  
81 2002b; Malinowski et al., 2020; Simpson et al., 2006), and fail to display normal cell  
82 heterogeneity known to influence metabolism (Benninger and Hodson, 2018; Benninger and  
83 Kravets, 2021; Nasteska et al., 2021). In addition, species-differences in islet cell composition  
84 and  $\beta$  cell function have been described (Cabrera et al., 2006; Hodson et al., 2013; Rodriguez-  
85 Diaz et al., 2011), yet their influence on energetics is still unclear. Lastly, bulk metabolomics  
86 has been informative for understanding  $\beta$  cell metabolism (Spegel et al., 2013; Wallace et al.,  
87 2013) and, while sensitive, lacks the resolution required to pinpoint glucose fate during  
88 glycolysis and the TCA cycle. Thus, our understanding of  $\beta$  cell glucose metabolism remains  
89 incomplete.

90 In the present study, we combine GC-MS-based  $^{13}\text{C}_6$  glucose tracing with the resolution of 2D  
91  $^1\text{H}$ - $^{13}\text{C}$  HSQC NMR multiplet analysis to map glucose fate in islets with high sensitivity. By  
92 applying this dual approach to human and mouse samples, we are able to provide a detailed  
93 cross-species depiction of glucose metabolism. By examining  $^{13}\text{C}$  labelling patterns, we  
94 confirm that PDH is the major contributor to the TCA cycle. We further show that pyruvate is  
95 directly converted to lactate in both human and mouse islets. However, lactate accumulation  
96 is much higher in human islets, which specifically express *LDHB* in the  $\beta$  cell compartment.  
97 We thus provide a detailed view of mouse and human islet metabolism, show that human  $\beta$   
98 cells generate significant lactate levels, and suggest that the role of lactate in  $\beta$  cell metabolism  
99 should be revisited.

100

101

102 **RESULTS**

103 **Glucose contribution to TCA cycle in human and mouse islets**

104 To investigate glucose handling, mouse and human islets were incubated overnight with  $^{13}\text{C}_6$   
105 glucose prior to metabolite extraction and GC-MS and 2D  $^1\text{H}, ^{13}\text{C}$  HSQC-NMR spectroscopy  
106 (**Figure 1A**). To allow sufficient glucose flux for detection of  $^{13}\text{C}$  incorporation into TCA  
107 metabolites, without inducing glucotoxicity, 10 mM  $^{13}\text{C}_6$  glucose was used. The incorporation  
108 of  $^{13}\text{C}$  from  $^{13}\text{C}_6$  glucose into the TCA cycle metabolites was then established via mass  
109 isotopologues distribution (MID) analysis (**Figure 1B**).

110 Suggesting a similar progression of glycolysis and the TCA cycle, glucose incorporation into  
111 the major metabolites malate, alanine and glutamate was not different between mouse and  
112 human islets (**Figure 1C-E**). However, a slight but significant increase in m+2/m+3 aspartate  
113 and fumarate was detected in mouse versus human islets (**Figure 1F and G**), reflecting an  
114 increased contribution of glucose-derived pyruvate into the TCA cycle via acetyl CoA. Total  
115 aspartate and alanine levels did not differ between the species (**Figure 1H and I**), whereas  
116 malate and fumarate levels (**Figure 1J and K**) were decreased in mouse. Glutamate levels  
117 were ~3-fold higher in mouse versus human islets, despite similar MIDs, implying that there is  
118 a larger contribution of non-labelled glutamate to the total glutamate pool in this species e.g.  
119 through glutamine transport (**Figure 1L**).

120 **Pyruvate management in human and mouse islets**

121 To obtain a higher definition view of pyruvate management, its contribution to the production  
122 of alanine and lactate was assessed. In both species, glucose incorporation could be detected  
123 in m+2 and m+3 lactate, likely derived from the TCA cycle and direct pyruvate conversion,  
124 respectively (**Figure 2A-C**). While the MID for alanine was similar in islets from both species  
125 (**Figure 1E**), the accumulation of m+ 2 and m+3 lactate was significantly (~ 6-fold) higher in  
126 humans (**Figure 2A**). In line with the larger size of human islets, or the increased proportion  
127 of  $\alpha$  cells, the total amount of lactate was higher in human than in mouse islets (**Figure 2B-**  
128 **D**).

129 While accumulation of m+2 lactate was expected, we were surprised to detect significant m+3  
130 lactate accumulation in human islets, since *Ldha* has been shown to be "disallowed" in mouse  
131  $\beta$  cells, hence preventing alternative fates for pyruvate (Ainscow et al., 2000; Pullen et al.,  
132 2010; Schuit et al., 2012; Sekine et al., 1994). However, recent studies in cancer cells have  
133 shown that pyruvate to lactate conversion is unaffected in single knockouts of LDHA and  
134 LDHB, and only in a double LDHA/B knockout is pyruvate no longer converted to lactate (Deng  
135 et al., 2022; Ždralević et al., 2018). Thus, LHDB can compensate for LDHA activity. Moreover,  
136 glucose-stimulated lactate production and oscillations were detected in intact mouse islets  
137 using a biosensor approach (Sdao et al., 2021). In accordance, we find that  $\beta$  cells  
138 predominantly and specifically express *LDHB* (**Figure 2E**). Moreover, we could not exclude  
139 the possibility that LDHA may also catalyze pyruvate to lactate conversion in  $\beta$  cells as they  
140 contain LDHA mRNA, albeit at low quantities, based on both single cell RNA-sequencing and  
141 bulk RNA-sequencing of FACS sorted  $\alpha$  cells and  $\beta$  cells (**Figure 2E and F**). This is consistent  
142 with the open chromatin conformation and transcription factor binding to this promoter in the  
143 human islet (**Figure 2G**).

144 **High resolution annotation of  $^{13}\text{C}_6$  glucose tracing data**

145 To identify isotopomer patterns with high-resolution, the MID analysis of  $^{13}\text{C}_6$  glucose-traced  
146 human and mouse islets was annotated with 2D  $^1\text{H}$ - $^{13}\text{C}$  HSQC NMR multiplet analysis. From  
147 uniformly labeled glucose,  $^{13}\text{C}$  atoms are incorporated into the metabolites of the TCA cycle  
148 through the activity of PDH and PC (**Figure 3A, B**). This leads to the formation of labeling  
149 patterns within the chemical structure of each metabolite that are specific to the pathway from  
150 which they are produced (**Figure 3A, B**). Therefore, the positions of  $^{13}\text{C}$  atoms within each  
151 metabolite can be utilized to elucidate the relative activities of PDH and PC. To define the  
152 different isotopomer patterns a numerical notation was used, where the numbers 0 and 1  
153 indicate  $^{12}\text{C}$  and  $^{13}\text{C}$  atoms, respectively. Confirming the accuracy of the approach, the  
154 accumulation of lactate<sub>111</sub> (i.e. fully-labeled lactate) was significantly higher in human  
155 compared to mouse islets, in line with the MID glucose-tracing data (**Figure 2A-C**) (**Figure**  
156 **3C-E**).

157 **TCA cycle depends more on PDH than PC flux in human and mouse islets**

158 In both human and mouse islets, lactate<sub>110</sub> made a greater contribution to the m+2  
159 isotopologue pool than the other possible isotopomers (**Figure 3C-E**). This finding suggests  
160 that lactate is produced from the oxidative TCA cycle rather than the reductive metabolism of  
161 PC-derived glutamate, from which pyruvate<sub>011</sub> and then lactate<sub>011</sub> would arise (**Figure 3C-E**).  
162 We also noticed that the majority of alanine was either 000 or 111, with only a very minor  
163 contribution to the other isotopomers (**Figure 3F-H**). As such, the labeled portion of alanine is  
164 produced from pyruvate upstream of the TCA cycle, meaning that the accumulation of  
165 pyruvate<sub>110</sub> from malate<sub>1100</sub> is mostly employed to regenerate lactate<sub>110</sub> (**Figure 3F-H**).  
166 Alanine<sub>111</sub> accumulation was slightly (~20%) higher in human than mouse islets, reflecting a  
167 greater contribution of transamination toward amino acid production (**Figure 3F-H**).  
168 Supporting the lactate isotopomer data, the contribution of  $^{13}\text{C}_6$  glucose to the labeling patterns  
169 of glutamate was found to be similar in humans and mice (**Figure 3I, J**). In both species, the  
170 most abundant labeled isotopomer was glutamate<sub>00011</sub> (**Figure 3I, J**), which is derived from  
171 TCA cycle flux through the activity of PDH (**Figure 3A, J**).

172 Together, these findings provide further evidence that pyruvate management in the pancreatic  
173  $\beta$  cell occurs primarily through PDH at the stimulatory glucose concentration used here (Alves  
174 et al., 2015; Lu et al., 2002a).

175

176 **DISCUSSION**

177 Using  $^{13}\text{C}_6$  glucose labeling coupled to GC-MS and 2D  $^1\text{H}$ - $^{13}\text{C}$  HSQC NMR spectroscopy, we  
178 have been able to obtain a high-resolution map of glucose fate within human and mouse islets.  
179 Unexpectedly, both human and mouse islets accumulate m+2 and m+3 lactate, meaning that  
180 lactate produced downstream of the TCA cycle (m+2) as well as via pyruvate  $\rightarrow$  lactate  
181 conversion (m+3) contribute equally to overall lactate production. However, pyruvate  $\rightarrow$  lactate  
182 conversion was much higher (~ 6-fold) in human compared to mouse islets, most likely due to  
183 the actions of LDHB. Finally, we show that labeled lactate and glutamate accumulate as  
184 lactate<sub>110</sub> and glutamate<sub>00011</sub>, confirming greater flux through PDH versus PC in both species.  
185 The major findings are schematically represented in **Figure 4**.

186 The observation that the islet lactate pool is derived from both TCA cycle- and pyruvate-  
187 derived sources suggests that mechanisms must be in place for direct pyruvate conversion,  
188 particularly in the human islet. In many tissues, pyruvate would be converted to lactate by  
189 LDH, however, the major *Ldha* subunit of the enzyme has been shown to be expressed at  
190 very low levels, disallowed or absent in the murine pancreatic  $\beta$  cell (Lemaire et al., 2016;  
191 Pullen et al., 2010; Sekine et al., 1994). Analysis of multiple published scRNA-seq datasets  
192 showed that *LDHA* is expressed in the human pancreatic  $\beta$  cell, albeit at much lower levels  
193 than in neighboring  $\alpha$  cells. It should be noted that the levels detected could represent  
194 contamination artefacts. In the presence of other LDH isoforms (*vide infra*), these relatively  
195 low levels of LDHA are likely sufficient to catalyze lactate production given the abundance of  
196 its substrate pyruvate in the  $\beta$  cell. Human  $\beta$  cells were also found to specifically and strongly  
197 express *LDHB*, which encodes the beta subunit of LDH. While an increased ratio of  
198 *LDHB*:*LDHA* is thought to catalyze production of pyruvate from lactate (Nam et al., 2016),  
199 recent studies have shown that *LDHB*-alone can replace the activity of LDHA to produce  
200 lactate. Indeed, deletion of both *LDHA* and *LDHB* is required to reduce lactate secretion in  
201 cells, whereas deletion of either *LDHA* or *LDHB* is without effect (Deng et al., 2022; Ždraljević  
202 et al., 2018).

203 Providing strong human genetic evidence for our findings here, studies have shown that  
204 Hyperinsulinemic hypoglycemic familial 7 (HHF7) patients develop exercise-induced  
205 hyperinsulinemia due to gain-of-function mutations in the cell surface lactate transporter  
206 MCT1/SLC16A1 (Otonkoski et al., 2007; Pullen et al., 2012). During exercise, when  
207 extracellular lactate levels are increased, cytoplasmic pyruvate accumulation is able to fuel  
208 the TCA cycle, leading to non glucose-dependent insulin release (Otonkoski et al., 2007;  
209 Pullen et al., 2012). To allow such lactate  $\rightarrow$  pyruvate conversion, human  $\beta$  cells must express  
210 sufficient LDH, and in particular *LDHB*, as shown here

211 It is also possible that other cell types within the islets, such as  $\alpha$ -cells, contribute to the  
212 accumulation of lactate. In particular, human  $\alpha$  cells account for ~35% of the entire islet and  
213 express *LDHA* at levels six times higher than  $\beta$  cells (Moin et al., 2020; Sanchez et al., 2021).  
214 However, a major source of  $\alpha$  cell lactate is via monocarboxylate transporters (Pullen and  
215 Rutter, 2013; Schuit et al., 2012; Zaborska et al., 2020), which are unlikely to play a role here  
216 as lactate was absent from the tracing medium. In addition, while the total amount of lactate  
217 was only doubled in humans compared to mice, the m+3 lactate accumulation was ~six-fold  
218 higher in human *versus* mouse islets. Taken together these data suggest that, although there  
219 might be a contribution of lactate from  $\alpha$  cells, this is unlikely to account for the whole m+3  
220 lactate increase detected here.

221 Human and mouse islets display a greater accumulation of lactate<sub>110</sub>, rather than lactate<sub>011</sub>.  
222 While the accumulation of lactate<sub>110</sub> is indistinguishable in the PDH- and PC-mediated TCA  
223 cycle, the 011 isotopomer would only derive from the reductive metabolism of PC-derived  
224 glutamate. Corroborating this, in islets from both species, the major glutamate isotopomer  
225 derived from exogenous <sup>13</sup>C<sub>6</sub> glucose was glutamate<sub>00011</sub>. Although glutamate is not a TCA  
226 cycle metabolite, it is in rapid exchange with α-KG and can be used as a read-out of TCA cycle  
227 flux through PDH or PC. Consequently, the accumulation of glutamate<sub>00011</sub> provides further  
228 evidence for a higher reliance of the TCA cycle on the activity of PDH, rather than PC.  
229 Although PC and PDH were thought to contribute equally to the TCA cycle in β-cells (Cline et  
230 al., 2004; Cline et al., 2011; Simpson et al., 2006), previous studies have shown that high  
231 glucose concentrations in vitro, more reflective of those seen post-prandially in vivo, are  
232 associated with an increase toward PDH activity (Alves et al., 2015; Lewandowski et al., 2020;  
233 Lu et al., 2002a). Our studies thus show that the relative contribution of PC to the TCA cycle  
234 is much lower than PDH (~20%), confirming findings from Alves et al in glucose-traced INS-1  
235 cells (Alves et al., 2015) and Lewandowski et al in human islets (Lewandowski et al., 2020).  
236 While anaplerosis through PC is relatively limited in the rβ cell, we note that glucose carbons  
237 can repeatedly transit the PEP cycle to generate ATP/ADP independently of oxidative  
238 phosphorylation (Lewandowski et al., 2020). As such, PC is able to make disproportionate  
239 contributions to K<sub>ATP</sub> channel closure, and hence the triggering phase of insulin secretion, by  
240 generating localized increases in ATP/ADP (Merrins et al., 2022). However, insulin secretion  
241 is not the only energy sink on the β cell, and glucose flux through PDH is likely to provide a  
242 source of glucose oxidation to support other demands such as continued insulin release and  
243 protein synthesis.

244 What might be the role of direct pyruvate to lactate conversion in pancreatic β cells? Since the  
245 action of LDH leads to oxidation of NADH to NAD<sup>+</sup>, lactate accumulation could provide a  
246 source of reducing equivalents to support other NADH-producing metabolic pathways.  
247 Providing evidence for a contribution of pyruvate to lactate conversion in NADH/NAD<sup>+</sup>  
248 balance, the alanine isotopomer distribution showed almost exclusively the accumulation of  
249 alanine<sub>000</sub> and alanine<sub>111</sub>. This finding suggests that the pyruvate accumulated downstream of  
250 the TCA cycle is mostly employed in the production of lactate<sub>110</sub>. Since the conversion of  
251 pyruvate to lactate is associated with the generation of cytosolic NAD<sup>+</sup>, higher levels of  
252 lactate<sub>111</sub> in humans might reflect an increase in the activity of NADH-producing pathways  
253 relative to rodents. However, β cells are thought to already have a large capacity to produce  
254 reducing equivalents, for example via the glycerol phosphate and malate-aspartate shuttles  
255 (Campbell and Newgard, 2021). Moreover, while LDH was found to form nanodomains with  
256 K<sub>ATP</sub> channels, supporting production of high local levels of NAD<sup>+</sup>, levels of lactate were  
257 insufficient to influence K<sub>ATP</sub> channel conductance (Ho et al., 2022). Lactate might be relatively  
258 more important when REDOX capacity is stretched, for example during ageing and ER stress,  
259 when NADH/NAD<sup>+</sup> pathways become more pronounced (Covarrubias et al., 2020). As such,  
260 future studies are warranted to investigate the functional impact of pyruvate to lactate  
261 conversion on β cell metabolism and function.

262 There are a number of limitations in the present studies. Firstly, <sup>13</sup>C<sub>6</sub> glucose labeling was  
263 conducted in whole islets rather than purified cell populations, excluding definitive annotation  
264 of β cell metabolism. However, since <sup>13</sup>C becomes diluted following achievement of steady-  
265 state, a large number (hundreds) of islets are required for accurate signal detection,  
266 particularly so for NMR. Secondly, the results are derived from male and female non-diabetic

267 donors, as well as male mouse islets. Going forwards, results should be stratified according  
268 to age, sex, BMI and T2D status, although we note that 800 MHz NMR capacity, probe time  
269 and helium availability largely preclude such experiments for the moment. Thirdly, whereas  
270 isotopologue and isotopomer data accurately delineate glucose fluxes and pyruvate  
271 management in islets, they are unable to measure the relative contribution of the identified  
272 pathways to insulin secretion. Nonetheless, our data provide a detailed and interrogable map  
273 of glucose metabolism pertaining to steady state insulin release in human and mouse islets,  
274 as well as other critical  $\beta$  cell housekeeping functions. Lastly, glucotoxicity might induce the  
275 upregulation of disallowed genes in  $\beta$ -cells (Bensellam et al., 2018). However, it is unlikely  
276 that the timings (12 hrs) and glucose concentration (10 mM) used here would overtly influence  
277 human  $\beta$ -cell lactate production, since *LDHA* or *LDHB* were not found to be differentially  
278 expressed in human islets exposed to 22.2 mM glucose for 4 days (Marselli et al., 2020).

279 In summary, by combining MID and multiplet analyses, we show that glucose makes a similar  
280 contribution to glycolysis and the TCA cycle in human and mouse islets. Furthermore, the  
281 isotopomer distribution confirms that, in both species, the relative activity of PDH is much  
282 higher than that of PC at elevated glucose concentration. However, the production of fully-  
283 labeled lactate was found to be significantly higher in human versus mouse islets, which is  
284 likely due to high expression levels of *LDHB*. Together, these results demonstrate that lactate  
285 production needs to be reconsidered in light of human beta cell metabolism and REDOX  
286 balance.

287 **METHODS**

288 **Ethics**

289 Animal studies were regulated by the Animals (Scientific Procedures) Act 1986 of the U.K.  
290 (Personal Project Licences P2ABC3A83 and PP1778740). Approval was granted by the  
291 University of Birmingham's Animal Welfare and Ethical Review Body (AWERB).

292 Human islets (Lille): human pancreatic tissues were harvested from brain-dead adult donors  
293 in accordance with the Lille clinical islet transplantation program's traceability requirements  
294 (clinicaltrials.gov, NCT01123187, NCT00446264, NCT01148680), and were approved in  
295 agreement with French regulations and the Ethical Committees of the University of Lille and  
296 the Centre Hospitalier Régional Universitaire de Lille.

297 Human islets (Milan): the use of human islets for research was approved by the Ethics  
298 Committee of San Raffaele Hospital in Milan (IPF002-2014).

299 Studies with human tissue were approved by the University of Birmingham Ethics Committee,  
300 the University of Oxford Ethics Committee, as well as the National Research Ethics Committee  
301 (REC reference 16/NE/0107, Newcastle and North Tyneside, UK).

302 **Mouse islets**

303 Male 8 to 12 week-old CD1 mice (Charles River stock no. 022) were used as tissue donors.  
304 Briefly, animals were culled using a schedule-1 method followed by injection of the common  
305 bile duct with 1 mg/mL collagenase NB 8 (Serva) in RPMI 1640 (Gibco) and pancreas  
306 dissection. After dissection, the pancreas was incubated in a water bath at 37°C for 12 min.  
307 Subsequently, the tissues were shaken in 15 mL of RPMI 1640 and centrifuged for 1 min at  
308 1500 rpm three times to induce mechanical digestion. Islets were separated using Histopaque-  
309 1119 and 1083 (Sigma-Aldrich) gradients, before hand-picking and culture. Unless otherwise  
310 stated, the islets obtained were kept in culture in RPMI 1640 supplemented with 10% fetal  
311 bovine serum (FBS, Gibco), 100 units/mL penicillin, and 100 µg/mL streptomycin (Sigma-  
312 Aldrich), at 37°C and 5% CO<sub>2</sub>.

313 **Human islets**

314 Islets were provided by the San Raffaele Diabetes Research Institute (DRI), Milan, Italy (ECIT  
315 Islet for Basic Research program), as well as the Translational Research for Diabetes at the  
316 University of Lille, Lille, France.

317 Upon receipt, the islets were cleared of possible debris via filtration with a 40 µm cut-off filter,  
318 hand-picked and cultured in CMRL medium (Corning) supplemented with 5.5 mM glucose  
319 (Sigma-Aldrich), 10% FBS, 100 units/mL penicillin, 100 µg/mL streptomycin and 0.1%  
320 amphotericin B (Sigma-Aldrich) at 37°C and 5% CO<sub>2</sub>. Donor characteristics are reported in  
321 Table 1.

322 **<sup>13</sup>C<sub>6</sub> glucose tracing**

323 For <sup>13</sup>C<sub>6</sub> glucose tracing, 60 (for GC-MS) or 150-230 (for NMR) islets were used. Isolated islets  
324 were cultured in RPMI 1640, no glucose medium (Gibco), supplemented with 10% BSA, 10%  
325 FBS, 100 units/mL penicillin, and 100 µg/mL streptomycin plus 10 mM <sup>13</sup>C<sub>6</sub> glucose (Sigma-

326 Aldrich). After 24 h, the metabolites were extracted adding HPLC-grade methanol, HPLC-  
327 grade distilled H<sub>2</sub>O containing 1 µg/mL D6-glutaric acid and HPLC-grade chloroform (all from  
328 Sigma-Aldrich) in a 1:1:1 ratio, to the islets. Following centrifugation, the polar fractions were  
329 collected and vacuum dried before either GC-MS or NMR analyses.

330 **GC-MS**

331 The dried polar extracts were prepared for GC-MS analysis through solubilization in 40 µL of  
332 2% methoxyamine hydrochloric acid in pyridine (Fisher Scientific) at 60°C for 60 min and  
333 derivatization with 60 µL of N-tertbutyldimethylsilyl-N-methyltrifluoroacetamide (MTBSTFA)  
334 with 1% tertbutyldimethyl-chlorosilane (TBDMCS) (both from Sigma-Aldrich). The suspension  
335 was further incubated at 60°C for 60 min, before being centrifuged at 13300 rpm for 10 min at  
336 4°C and transferred to chromatography vials with a glass insert (Restek) for GC-MS analysis.  
337 The samples were analyzed on an Agilent 8890 GC and 5977B MSD system. To do this, 1 µL  
338 of sample was injected in splitless mode with helium carrier gas at a rate of 1.0 mL/min. The  
339 compound detection was carried out in scan mode and total ion counts of each metabolite  
340 were normalized to the internal standard D6-glutaric acid using an in-house MATLAB script.

341 **NMR spectroscopy**

342 Following the <sup>13</sup>C<sub>6</sub> glucose tracing, the dried polar metabolites were resuspended in 60 µL of  
343 phosphate buffer: 57.8 mM disodium phosphate (Na<sub>2</sub>HPO<sub>4</sub>, Sigma-Aldrich), 42.2 mM  
344 monosodium phosphate (NaH<sub>2</sub>PO<sub>4</sub>, Sigma-Aldrich), 0.5 mM 3-(trimethylsilyl)  
345 2,2,3,3-d4 acid sodium salt (D4-TMSP, Sigma-Aldrich) in deuterium oxide (D<sub>2</sub>O, Sigma-  
346 Aldrich). Subsequently, the samples were centrifuged for 10 min at 14800 rpm and sonicated  
347 in an ultrasonic bath for 5 min, before being loaded into NMR tubes (outer diameter: 1.7 mm,  
348 Bruker) for acquisition. A Bruker Neo 800 MHz NMR spectrometer equipped with a 1.7 mm z-  
349 PFG TCI Cryoprobe was used to acquire 2D <sup>1</sup>H, <sup>13</sup>C-HSQC NMR spectra. The HSQC spectra  
350 were acquired with echo/anti-echo gradient coherence selection with an additional pre-  
351 saturation for suppressing the residual water resonance. The spectral widths were 15.6298  
352 ppm and 189.7832 ppm in the <sup>1</sup>H and <sup>13</sup>C dimension, 512 complex data points were acquired  
353 for the <sup>1</sup>H dimension and 25% (512) out of 2048 complex data points were acquired for the  
354 <sup>13</sup>C indirect dimension using a non-uniform sampling scheme. Apparent <sup>13</sup>C, <sup>13</sup>C J-coupling  
355 was enhanced four-fold. The interscan relaxation delay was set to 1.5 s. 2D <sup>1</sup>H, <sup>13</sup>C-HSQC  
356 spectra were reconstructed via the compressed sensing IRLS algorithm using the MDDNMR  
357 (version 2.5) (Kazimierczuk and Orekhov, 2011) and NMRPipe (version 9.2) (Delaglio et al.,  
358 1995) software. All NMR spectra were analysed in the MATLAB based MetaboLab software  
359 package (Ludwig and Günther, 2011).

360 **Transcriptomics analysis**

361 Quantification data for all published scRNA-seq datasets were kindly provided by Leon Van  
362 Gorp (van Gorp et al., 2022). In brief, pseudo-counts were normalized for each data set using  
363 Seurat (Satija et al., 2015), and the cell identity was assigned based on the requirement for  
364 hormone gene expression to be in the top 1% expressed genes in each cell using Aucell (Aibar  
365 et al., 2017). Quantification for published FACS sorted alpha and β cells were obtained from  
366 GEO database repository under Arda et al (Arda et al., 2016). The raw read files for each cell  
367 type were merged, trimmed and the transcripts were quantified using Kallisto (Bray et al.,

368 2016) or aligned and quantified as previously described (Akerman et al., 2020), with similar  
369 results.

370 **Statistics and reproducibility**

371 Statistical significance was assessed with GraphPad Prism 9 (version 9.2.0). Pairwise  
372 comparisons were made using Welch's test (assuming non-equal standard deviation between  
373 groups). Multiple interactions were determined using one-way ANOVA or two-way ANOVA,  
374 with Sidak's post-hoc test.

375 All error bars represent mean  $\pm$  S.E.M. and a p-value less than 0.05 was considered  
376 significant: \*p< 0.05; \*\*p< 0.01; \*\*\*p< 0.001, \*\*\*\*p<0.0001.

377

378 **AUTHOR CONTRIBUTIONS**

379 F.C. performed experiments, analysed data and wrote the manuscript. D.N. and H.R.M.  
380 performed experiments. Z.J. and I.A. performed bioinformatic analysis. R.N., L.P., C.B., F.P.  
381 and J.K-C. isolated and provided human islets. C.L. performed  $^1\text{H}, ^{13}\text{C}$ -HSQC NMR  
382 experiments and analysis. G.G.L., D.T. and J.R. ran GC-MS on  $^{13}\text{C}_6$  glucose labelled samples  
383 and provided analysis. D.J.H. supervised the studies, provided analysis and wrote the  
384 manuscript with contributions from C.L. and D.T. All authors read and approved the studies.

385 **ACKNOWLEDGEMENTS**

386 D.J.H. was supported by MRC (MR/N00275X/1 and MR/S025618/1) and Diabetes UK  
387 (17/0005681) Project Grants, as well as a UKRI ERC Frontier Research Guarantee Grant  
388 (EP/X026833/1). This project has received funding from the European Research Council  
389 (ERC) under the European Union's Horizon 2020 research and innovation programme  
390 (Starting Grant 715884 to D.J.H.). G.G.L. was supported by a Wellcome Trust Senior  
391 Fellowship (104612/Z/14/Z). D.T. was supported by a Cancer Research UK Programme Grant  
392 (C42109/A24747). The research was funded by the National Institute for Health Research  
393 (NIHR) Oxford Biomedical Research Centre (BRC). The views expressed are those of the  
394 author(s) and not necessarily those of the NHS, the NIHR or the Department of Health. We  
395 would like to acknowledge the support and resources of the Birmingham Metabolic Tracer  
396 Analysis Core. We thank Dr. Matthew J. Merrins (University of Wisconsin) for critical  
397 comments on the manuscript.

398 **DISCLOSURE STATEMENT**

399 D.J.H. receives licensing revenue from Celtryns Research.

400

401 **REFERENCES**

402

403 Aibar, S., Gonzalez-Blas, C.B., Moerman, T., Huynh-Thu, V.A., Imrichova, H., Hulselmans, G., Rambow, F., Marine, J.C., Geurts, P., Aerts, J., et al. (2017). SCENIC: single-cell regulatory network inference and clustering. *Nat Methods* 14, 1083-1086.

404

405 Ainscow, E.K., Zhao, C., and Rutter, G.A. (2000). Acute overexpression of lactate dehydrogenase-A perturbs beta-cell mitochondrial metabolism and insulin secretion. *Diabetes* 49, 1149-1155.

406

407 Akerman, I., Kasaai, B., Bazarova, A., Sang, P.B., Peiffer, I., Artufel, M., Derelle, R., Smith, G., Rodriguez-Martinez, M., Romano, M., et al. (2020). A predictable conserved DNA base composition signature defines human core DNA replication origins. *Nat Commun* 11, 4826.

408

409 Akerman, I., Tu, Z., Beucher, A., Rolando, D.M.Y., Sauty-Colace, C., Benazra, M., Nakic, N., Yang, J., Wang, H., Pasquali, L., et al. (2017). Human Pancreatic beta Cell lncRNAs Control Cell-Specific Regulatory Networks. *Cell Metab* 25, 400-411.

410

411 Alves, T.C., Pongratz, R.L., Zhao, X., Yarborough, O., Sereda, S., Shirihai, O., Cline, G.W., Mason, G., and Kibbey, R.G. (2015). Integrated, Step-Wise, Mass-Isotopomeric Flux Analysis of the TCA Cycle. *Cell Metab* 22, 936-947.

412

413 Arda, H.E., Li, L., Tsai, J., Torre, E.A., Rosli, Y., Peiris, H., Spitale, R.C., Dai, C., Gu, X., Qu, K., et al. (2016). Age-Dependent Pancreatic Gene Regulation Reveals Mechanisms Governing Human beta Cell Function. *Cell Metab* 23, 909-920.

414

415 Benninger, R.K.P., and Hodson, D.J. (2018). New Understanding of  $\beta$ -Cell Heterogeneity and In Situ Islet Function. *Diabetes* 67, 537-547.

416

417 Benninger, R.K.P., and Kravets, V. (2021). The physiological role of  $\beta$ -cell heterogeneity in pancreatic islet function. *Nature Reviews Endocrinology*.

418

419 Bensellam, M., Jonas, J.C., and Laybutt, D.R. (2018). Mechanisms of beta-cell dedifferentiation in diabetes: recent findings and future research directions. *J Endocrinol* 236, R109-R143.

420

421 Bray, N.L., Pimentel, H., Melsted, P., and Pachter, L. (2016). Near-optimal probabilistic RNA-seq quantification. *Nat Biotechnol* 34, 525-527.

422

423 Cabrera, O., Berman, D.M., Kenyon, N.S., Ricordi, C., Berggren, P.O., and Caicedo, A. (2006). The unique cytoarchitecture of human pancreatic islets has implications for islet cell function. *Proceedings of the National Academy of Sciences of the United States of America* 103, 2334-2339.

424

425 Campbell, J.E., and Newgard, C.B. (2021). Mechanisms controlling pancreatic islet cell function in insulin secretion. *Nat Rev Mol Cell Biol* 22, 142-158.

426

427 Cline, G.W., Lepine, R.L., Papas, K.K., Kibbey, R.G., and Shulman, G.I. (2004).  $^{13}\text{C}$  NMR isotopomer analysis of anaplerotic pathways in INS-1 cells. *J Biol Chem* 279, 44370-44375.

428

429 Cline, G.W., Pongratz, R.L., Zhao, X., and Papas, K.K. (2011). Rates of insulin secretion in INS-1 cells are enhanced by coupling to anaplerosis and Kreb's cycle flux independent of ATP synthesis. *Biochem Biophys Res Commun* 415, 30-35.

430

431 Covarrubias, A.J., Perrone, R., Grozio, A., and Verdin, E. (2020). NAD $^+$  metabolism and its roles in cellular processes during ageing. *Nature Reviews Molecular Cell Biology* 22, 119-141.

432

433 De Vos, A., Heimberg, H., Quartier, E., Huypens, P., Bouwens, L., Pipeleers, D., and Schuit, F. (1995). Human and rat beta cells differ in glucose transporter but not in glucokinase gene expression. *Journal of Clinical Investigation* 96, 2489-2495.

434

435 Delaglio, F., Grzesiek, S., Vuister, G., Zhu, G., Pfeifer, J., and Bax, A. (1995). NMRPipe: A multidimensional spectral processing system based on UNIX pipes. *Journal of Biomolecular NMR* 6.

436

437 Deng, H., Gao, Y., Trappetti, V., Hertig, D., Karatkevich, D., Losmanova, T., Urzi, C., Ge, H., Geest, G.A., Bruggmann, R., et al. (2022). Targeting lactate dehydrogenase B-dependent mitochondrial metabolism affects tumor initiating cells and inhibits tumorigenesis of non-small cell lung cancer by inducing mtDNA damage. *Cellular and Molecular Life Sciences* 79.

438

439 Enge, M., Arda, H.E., Mignardi, M., Beausang, J., Bottino, R., Kim, S.K., and Quake, S.R. (2017). Single-Cell Analysis of Human Pancreas Reveals Transcriptional Signatures of Aging and Somatic Mutation Patterns. *Cell* 171, 321-330 e314.

440

441

442

443

444

445

446

447

448

449

450

451

452

453

454

455

456 Ferdaoussi, M., Dai, X., Jensen, M.V., Wang, R., Peterson, B.S., Huang, C., Ilkayeva, O.,  
457 Smith, N., Miller, N., Hajmrle, C., et al. (2015). Isocitrate-to-SENP1 signaling amplifies insulin  
458 secretion and rescues dysfunctional beta cells. *J Clin Invest* 125, 3847-3860.

459 Foster, H.R., Ho, T., Potapenko, E., Sdao, S.M., Huang, S.M., Lewandowski, S.L.,  
460 VanDeusen, H.R., Davidson, S.M., Cardone, R.L., Prentki, M., et al. (2022).  $\beta$ -cell deletion of  
461 the PKm1 and PKm2 isoforms of pyruvate kinase in mice reveals their essential role as  
462 nutrient sensors for the KATP channel. *eLife* 11.

463 Henquin, J.C. (2000). Triggering and amplifying pathways of regulation of insulin secretion by  
464 glucose. *Diabetes* 49, 1751-1760.

465 Ho, T., Potapenko, E., Davis, D.B., and Merrins, M.J. (2022). A plasma membrane-associated  
466 glycolytic metabolon is functionally coupled to KATP channels in pancreatic  $\alpha$  and  $\beta$  cells from  
467 humans and mice. *bioRxiv*.

468 Hodson, D.J., Mitchell, R.K., Bellomo, E.A., Sun, G., Vinet, L., Meda, P., Li, D., Li, W.H.,  
469 Bugliani, M., Marchetti, P., et al. (2013). Lipotoxicity disrupts incretin-regulated human beta  
470 cell connectivity. *Journal of Clinical Investigation* 123, 4182-4194.

471 Kazimierczuk, K., and Orekhov, V.Y. (2011). Accelerated NMR Spectroscopy by Using  
472 Compressed Sensing. *Angewandte Chemie International Edition* 50, 5556-5559.

473 Lawlor, N., George, J., Bolisetty, M., Kursawe, R., Sun, L., Sivakamasundari, V., Kycia, I.,  
474 Robson, P., and Stitzel, M.L. (2017). Single-cell transcriptomes identify human islet cell  
475 signatures and reveal cell-type-specific expression changes in type 2 diabetes. *Genome  
476 Research* 27, 208-222.

477 Lemaire, K., Thorrez, L., and Schuit, F. (2016). Disallowed and Allowed Gene Expression:  
478 Two Faces of Mature Islet Beta Cells. *Annu Rev Nutr* 36, 45-71.

479 Lewandowski, S.L., Cardone, R.L., Foster, H.R., Ho, T., Potapenko, E., Poudel, C.,  
480 VanDeusen, H.R., Sdao, S.M., Alves, T.C., Zhao, X., et al. (2020). Pyruvate Kinase Controls  
481 Signal Strength in the Insulin Secretory Pathway. *Cell Metabolism* 32, 736-750.e735.

482 Lu, Mulder, H., Zhao, P., Burgess, S.C., Jensen, M.V., Kamzolova, S., Newgard, C.B., and  
483 Sherry, A.D. (2002a).  $^{13}\text{C}$  NMR isotopomer analysis reveals a connection between pyruvate  
484 cycling and glucose-stimulated insulin secretion (GSIS). *Proc Natl Acad Sci U S A* 99, 2708-  
485 2713.

486 Lu, D., Mulder, H., Zhao, P., Burgess, S.C., Jensen, M.V., Kamzolova, S., Newgard, C.B., and  
487 Sherry, A.D. (2002b).  $^{13}\text{C}$  NMR isotopomer analysis reveals a connection between pyruvate  
488 cycling and glucose-stimulated insulin secretion (GSIS). *Proc Natl Acad Sci U S A* 99, 2708-  
489 2713.

490 Ludwig, C., and Günther, U.L. (2011). MetaboLab - advanced NMR data processing and  
491 analysis for metabolomics. *BMC Bioinformatics* 12.

492 Malinowski, R.M., Ghiasi, S.M., Mandrup-Poulsen, T., Meier, S., Lerche, M.H., Ardenkjær-  
493 Larsen, J.H., and Jensen, P.R. (2020). Pancreatic  $\beta$ -cells respond to fuel pressure with an  
494 early metabolic switch. *Scientific Reports* 10.

495 Marselli, L., Piron, A., Suleiman, M., Colli, M.L., Yi, X., Khamis, A., Carrat, G.R., Rutter, G.A.,  
496 Bugliani, M., Giusti, L., et al. (2020). Persistent or Transient Human  $\beta$  Cell Dysfunction Induced  
497 by Metabolic Stress: Specific Signatures and Shared Gene Expression with Type 2 Diabetes.  
498 *Cell Reports* 33.

499 Merrins, M.J., Corkey, B.E., Kibbey, R.G., and Prentki, M. (2022). Metabolic cycles and signals  
500 for insulin secretion. *Cell Metabolism* 34, 947-968.

501 Moin, A.S.M., Cory, M., Gurlo, T., Saisho, Y., Rizza, R.A., Butler, P.C., and Butler, A.E. (2020).  
502 Pancreatic alpha-cell mass across adult human lifespan. *Eur J Endocrinol* 182, 219-231.

503 Nam, K., Oh, S., and Shin, I. (2016). Ablation of CD44 induces glycolysis-to-oxidative  
504 phosphorylation transition via modulation of the c-Src-Akt-LKB1-AMPKalpha pathway.  
505 *Biochem J* 473, 3013-3030.

506 Nasteska, D., Fine, N.H.F., Ashford, F.B., Cuozzo, F., Viloria, K., Smith, G., Dahir, A., Dawson,  
507 P.W.J., Lai, Y.-C., Bastidas-Ponce, A., et al. (2021). PDX1LOW MAFALOW  $\beta$ -cells contribute  
508 to islet function and insulin release. *Nature Communications* 12, 674.

509 Otonkoski, T., Jiao, H., Kaminen-Ahola, N., Tapia-Paez, I., Ullah, M.S., Parton, L.E., Schuit,  
510 F., Quintens, R., Sipila, I., Mayatepek, E., et al. (2007). Physical exercise-induced

511 hypoglycemia caused by failed silencing of monocarboxylate transporter 1 in pancreatic beta  
512 cells. *American Journal of Human Genetics* 81, 467-474.

513 Pullen, T.J., Khan, A.M., Barton, G., Butcher, S.A., Sun, G., and Rutter, G.A. (2010).  
514 Identification of genes selectively disallowed in the pancreatic islet. *Islets* 2, 89-95.

515 Pullen, T.J., and Rutter, G.A. (2013). When less is more: the forbidden fruits of gene  
516 repression in the adult beta-cell. *Diabetes Obes Metab* 15, 503-512.

517 Pullen, T.J., Sylow, L., Sun, G., Halestrap, A.P., Richter, E.A., and Rutter, G.A. (2012).  
518 Overexpression of Monocarboxylate Transporter-1 (Slc16a1) in Mouse Pancreatic beta-Cells  
519 Leads to Relative Hyperinsulinism During Exercise. *Diabetes* 61, 1719-1725.

520 Rodriguez-Diaz, R., Dando, R., Jacques-Silva, M.C., Fachado, A., Molina, J., Abdulreda,  
521 M.H., Ricordi, C., Roper, S.D., Berggren, P.O., and Caicedo, A. (2011). Alpha cells secrete  
522 acetylcholine as a non-neuronal paracrine signal priming beta cell function in humans. *Nature  
523 Medicine* 17, 888-892.

524 Rorsman, P., and Ashcroft, F.M. (2018). Pancreatic beta-Cell Electrical Activity and Insulin  
525 Secretion: Of Mice and Men. *Physiol Rev* 98, 117-214.

526 Rutter, G.A., Pullen, T.J., Hodson, D.J., and Martinez-Sanchez, A. (2015). Pancreatic beta-  
527 cell identity, glucose sensing and the control of insulin secretion. *Biochem J* 466, 203-218.

528 Sanchez, P.K.M., Khazaei, M., Gatineau, E., Geravandi, S., Lupse, B., Liu, H., Dringen, R.,  
529 Wojtusciszyn, A., Gilon, P., Maedler, K., et al. (2021). LDHA is enriched in human islet alpha  
530 cells and upregulated in type 2 diabetes. *Biochem Biophys Res Commun* 568, 158-166.

531 Satija, R., Farrell, J.A., Gennert, D., Schier, A.F., and Regev, A. (2015). Spatial reconstruction  
532 of single-cell gene expression data. *Nat Biotechnol* 33, 495-502.

533 Schuit, F., Van Lommel, L., Granvik, M., Goyvaerts, L., de Faudeur, G., Schraenen, A., and  
534 Lemaire, K. (2012). beta-cell-specific gene repression: a mechanism to protect against  
535 inappropriate or maladjusted insulin secretion? *Diabetes* 61, 969-975.

536 Sdao, S.M., Ho, T., Poudel, C., Foster, H.R., De Leon, E.R., Adams, M.T., Lee, J.H., Blum,  
537 B., Rane, S.G., and Merrins, M.J. (2021). CDK2 limits the highly energetic secretory program  
538 of mature beta cells by restricting PEP cycle-dependent K(ATP) channel closure. *Cell Rep* 34,  
539 108690.

540 Segerstolpe, Å., Palasantza, A., Eliasson, P., Andersson, E.-M., Andréasson, A.-C., Sun, X.,  
541 Picelli, S., Sabirsh, A., Clausen, M., Bjursell, M.K., et al. (2016). Single-Cell Transcriptome  
542 Profiling of Human Pancreatic Islets in Health and Type 2 Diabetes. *Cell Metabolism* 24, 593-  
543 607.

544 Sekine, N., Cirulli, V., Regazzi, R., Brown, L.J., Gine, E., Tamarit-Rodriguez, J., Girotti, M.,  
545 Marie, S., MacDonald, M.J., Wollheim, C.B., et al. (1994). Low lactate dehydrogenase and  
546 high mitochondrial glycerol phosphate dehydrogenase in pancreatic beta-cells. Potential role  
547 in nutrient sensing. *Journal of Biological Chemistry* 269, 4895-4902.

548 Simpson, N.E., Khokhlova, N., Oca-Cossio, J.A., and Constantinidis, I. (2006). Insights into  
549 the role of anaplerosis in insulin secretion: A <sup>13</sup>C NMR study. *Diabetologia* 49, 1338-1348.

550 Spegel, P., Sharoyko, V.V., Goehring, I., Danielsson, A.P., Malmgren, S., Nagorny, C.L.,  
551 Andersson, L.E., Koeck, T., Sharp, G.W., Straub, S.G., et al. (2013). Time-resolved  
552 metabolomics analysis of beta-cells implicates the pentose phosphate pathway in the control  
553 of insulin release. *Biochem J* 450, 595-605.

554 Thorens, B., Sarkar, H.K., Kaback, H.R., and Lodish, H.F. (1988). Cloning and functional  
555 expression in bacteria of a novel glucose transporter present in liver, intestine, kidney, and  
556 beta-pancreatic islet cells. *Cell* 55, 281-290.

557 van Gurp, L., Fodoulian, L., Oropeza, D., Furuyama, K., Bru-Tari, E., Vu, A.N., Kaddis, J.S.,  
558 Rodriguez, I., Thorel, F., and Herrera, P.L. (2022). Generation of human islet cell type-specific  
559 identity genesets. *Nat Commun* 13, 2020.

560 Wallace, M., Whelan, H., and Brennan, L. (2013). Metabolomic analysis of pancreatic beta  
561 cells following exposure to high glucose. *Biochimica et Biophysica Acta (BBA) - General  
562 Subjects* 1830, 2583-2590.

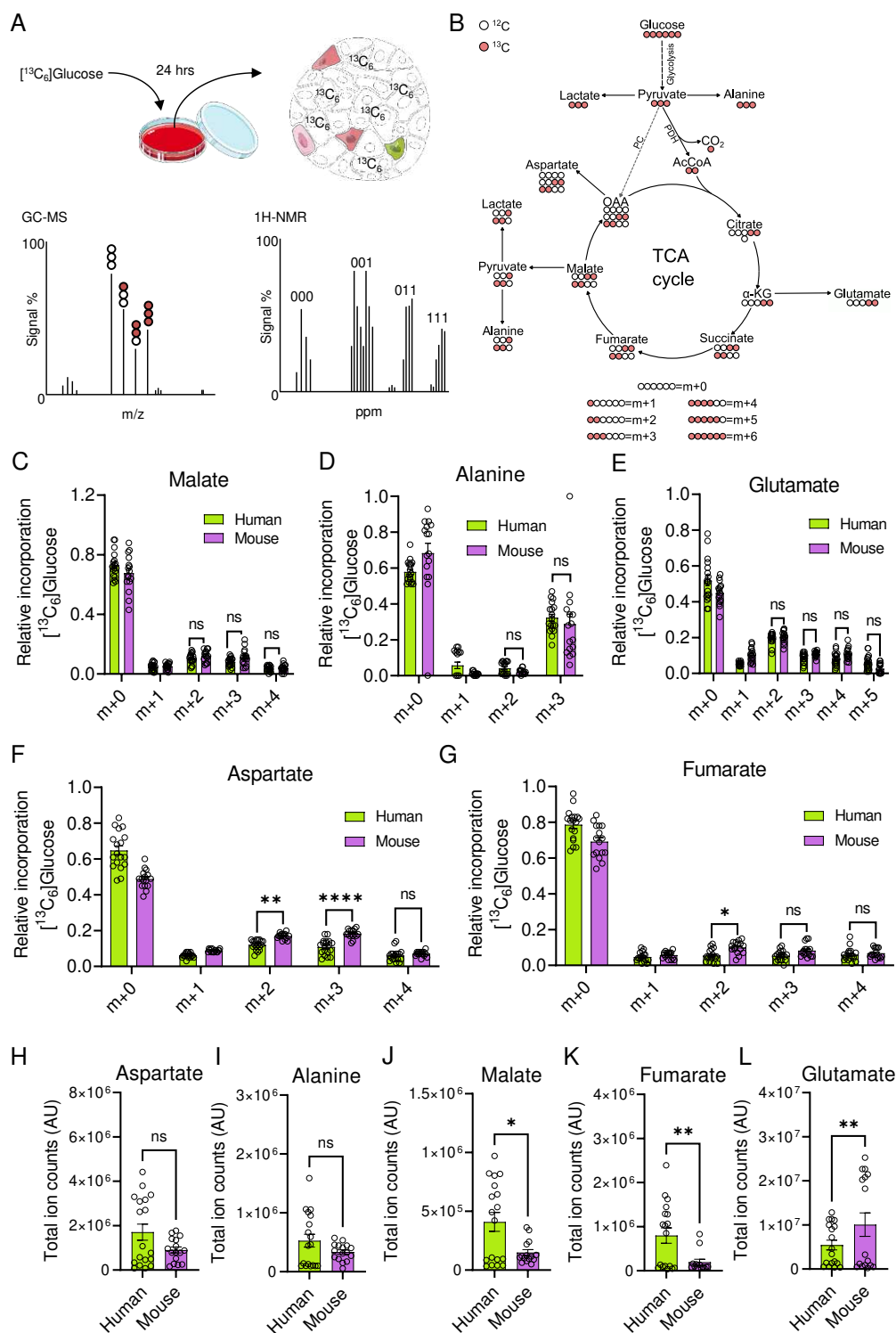
563 Wang, Y.J., Schug, J., Won, K.J., Liu, C., Naji, A., Avrahami, D., Golson, M.L., and Kaestner,  
564 K.H. (2016). Single-Cell Transcriptomics of the Human Endocrine Pancreas. *Diabetes* 65,  
565 3028-3038.

566 Xin, Y., Gutierrez, G.D., Okamoto, H., Kim, J., Lee, A.H., Adler, C., Ni, M., Yancopoulos, G.D.,  
567 Murphy, A.J., and Gromada, J. (2018). Pseudotime Ordering of Single Human beta-Cells  
568 Reveals States of Insulin Production and Unfolded Protein Response. *Diabetes*.  
569 Zaborska, K.E., Dadi, P.K., Dickerson, M.T., Nakhe, A.Y., Thorson, A.S., Schaub, C.M., Graff,  
570 S.M., Stanley, J.E., Kondapavuluru, R.S., Denton, J.S., et al. (2020). Lactate activation of  
571 alpha-cell KATP channels inhibits glucagon secretion by hyperpolarizing the membrane  
572 potential and reducing  $\text{Ca}^{2+}$  entry. *Mol Metab* 42, 101056.  
573 Ždrálević, M., Brand, A., Di Ianni, L., Dettmer, K., Reinders, J., Singer, K., Peter, K., Schnell,  
574 A., Bruss, C., Decking, S.-M., et al. (2018). Double genetic disruption of lactate  
575 dehydrogenases A and B is required to ablate the “Warburg effect” restricting tumor growth to  
576 oxidative metabolism. *Journal of Biological Chemistry* 293, 15947-15961.

577

578

579 **FIGURES AND FIGURE LEGENDS**

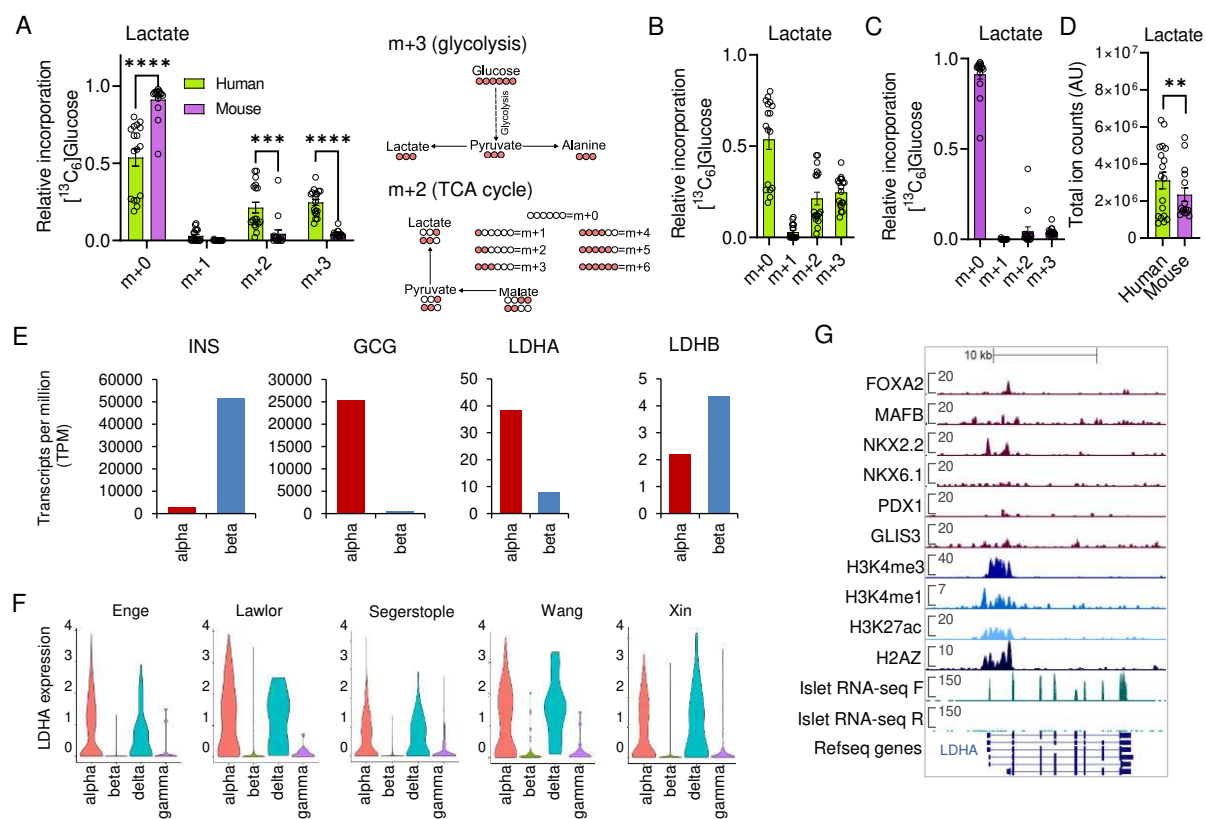


580  
581 **Figure 1: MID analysis of glucose fate in human and mouse islets. A)** Schematic showing  
582 GC-MS and <sup>1</sup>H-NMR-based <sup>13</sup>C<sub>6</sub> glucose-tracing protocol in primary islets. **B)** Schematic showing mass  
583 isotopomer distribution (MID) analysis of <sup>13</sup>C<sub>6</sub> glucose-tracing data. **C-E)** MID analysis showing similar incorporation of <sup>13</sup>C from <sup>13</sup>C<sub>6</sub> glucose into malate (C), alanine (D) and glutamate (E) in human and mouse islets. **F, G)** MID analysis showing increased incorporation of <sup>13</sup>C from <sup>13</sup>C<sub>6</sub> glucose into m+2 aspartate (F), and m+2 and m+3 fumarate (G) in mouse compared to human islets. **H, I)** Total amount of extracted aspartate (H) and alanine (I) is similar in human and mouse islets. **(J-L)** Total amount of extracted malate (J) and

589 fumarate (K) is decreased in mouse relative to human islets, whereas glutamate (L) is  
590 increased. For all data, n = 18 independent replicates from 9 human donors; n = 10 islet  
591 preparations from 15 animals. C-G were analyzed using two-way ANOVA and Sidak's post-  
592 hoc test. H-L were analyzed using Welch's test. Bar graphs show individual datapoints and  
593 mean  $\pm$  SEM. AU = arbitrary unit.

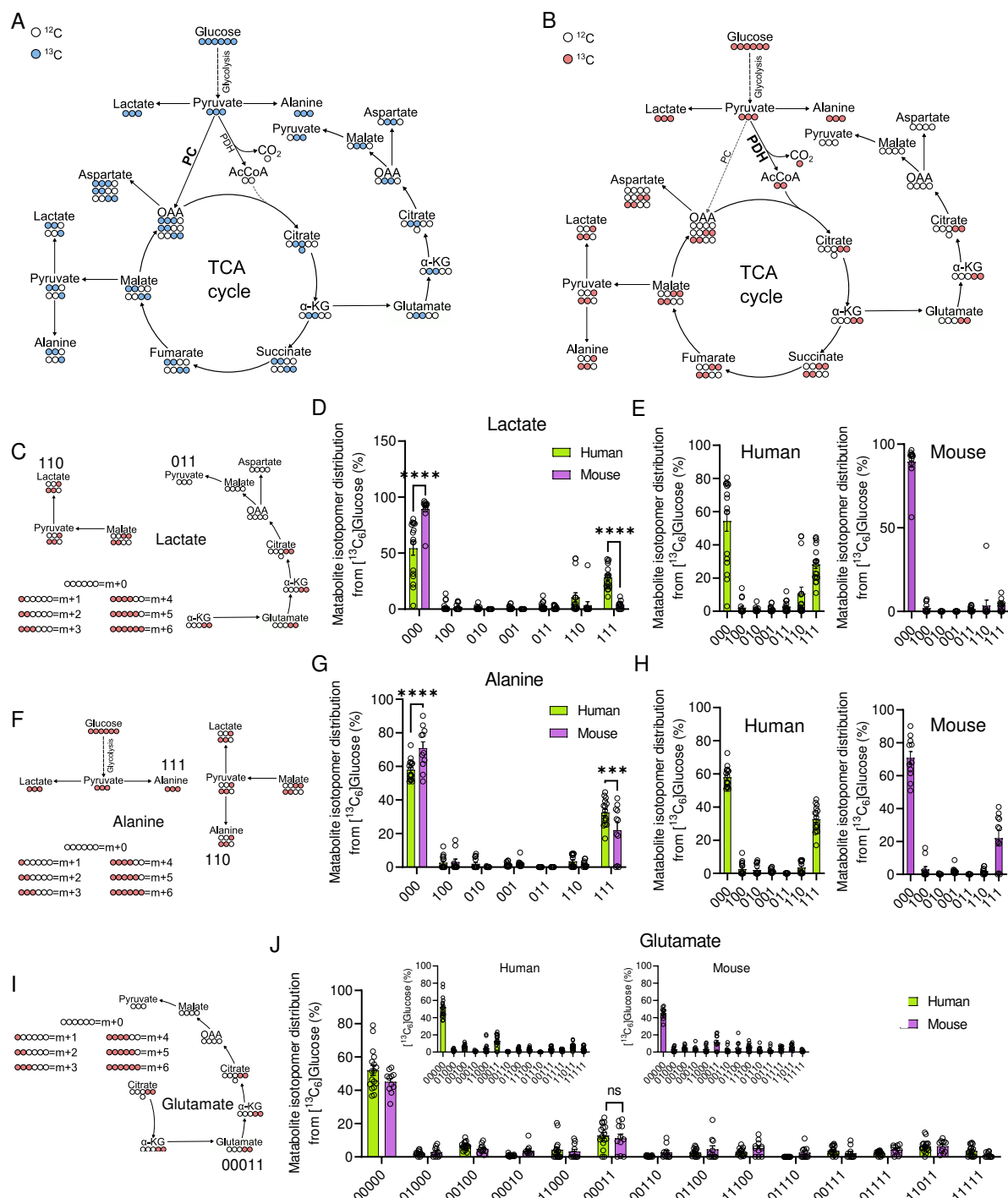
594

595



596  
597 **Figure 2: Human and mouse islets convert pyruvate to lactate. A-C)** MID analysis shows  
598 detectable glucose incorporation into m+2 (TCA cycle) and m+3 (pyruvate conversion) lactate,  
599 with more accumulation in human (A, B) versus mouse (A, C) islets. **D)** Total lactate production  
600 is higher in human compared to mouse islets. **E)** Normalized mRNA levels (transcripts per  
601 million, TPM) for *INS*, *GCG*, *LDHA* and *LDHB* genes in fluorescent-activated cell-sorted  
602 (FACS) alpha and β cell samples (re-analysis of data from (Arda et al., 2016)). **F)** Normalized  
603 LDHA expression in α, β, δ and γ cells from five independent human islet single cell RNA-  
604 sequencing experiments (Enge et al., 2017; Lawlor et al., 2017; Segerstolpe et al., 2016;  
605 Wang et al., 2016; Xin et al., 2018). Data from each study was subjected to re-assignment of  
606 cell identity based upon strict criteria (see Methods). **G)** Genome browser snapshot of  
607 transcription factor binding, histone modification (ChIP-seq, targets as indicated) and RNA-  
608 sequencing experiments performed on human islets (Akerman et al., 2017). Scales represent  
609 RPKM. For A-D, n = 18 independent replicates from 9 human donors; n = 10 islet preparations  
610 from 15 animals. A was analyzed using two-way ANOVA and Sidak's post-hoc test. D was  
611 analyzed using Welch's test. Bar graphs show individual datapoints and mean ± SEM. AU =  
612 arbitrary unit.

613  
614



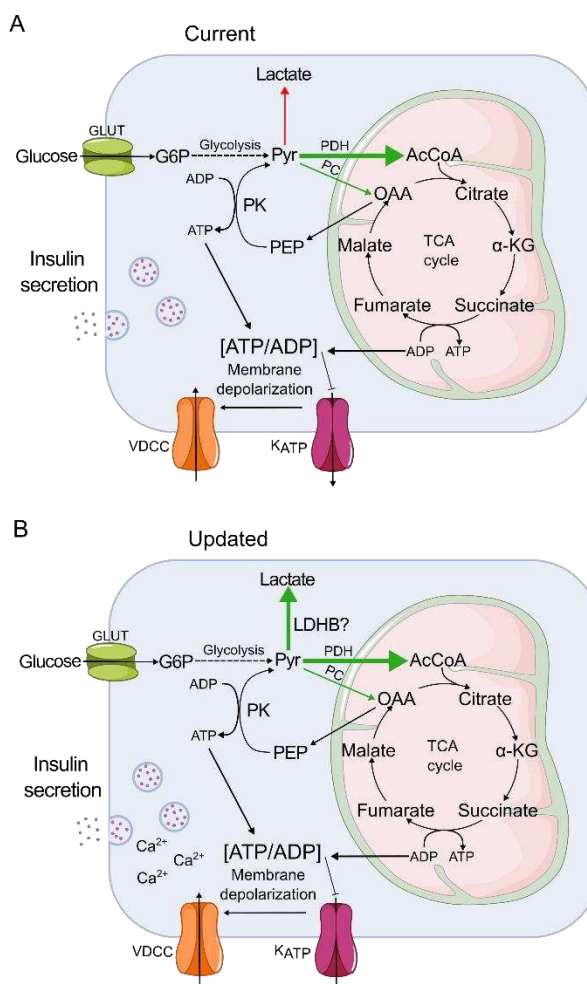
615

616 **Figure 3: Incorporation of <sup>13</sup>C from <sup>13</sup>C<sub>6</sub> glucose into TCA cycle metabolites through**  
 617 **PDH and PC.** **A)** White and blue circles, respectively, show the incorporation of <sup>12</sup>C and <sup>13</sup>C  
 618 into TCA cycle metabolites arising from metabolism of pyruvate by PC. **B)** White and red  
 619 circles, respectively, represent <sup>12</sup>C and <sup>13</sup>C atoms as incorporated from <sup>13</sup>C<sub>6</sub> glucose into the  
 620 TCA cycle through the conversion of pyruvate to acetyl-CoA by PDH. **C-E)** Lactate<sub>000</sub>,  
 621 lactate<sub>111</sub> and lactate<sub>110</sub> are the most abundant isotopomers (C) in both humans and mice (D),  
 622 although the incorporation of <sup>13</sup>C from <sup>13</sup>C<sub>6</sub> glucose into lactate<sub>111</sub> is significantly higher in  
 623 human than mouse islets (D, E). **F-H)** <sup>13</sup>C incorporation into alanine isotopomers (F) is similar  
 624 in human and mouse islets (G), with alanine<sub>111</sub> being the most represented labeled isotopomer  
 625 (G, H). **I, J)** The distribution of labeling patterns for glutamate (I) are similar in human and

626 mouse islets (J), with glutamate<sub>00011</sub> being the most abundant labeled isotopomer in both  
627 species (J). For all data, n = 16-17 islet preparations, 9 human donors and n = 7-8 islet  
628 preparations, 12-15 animals. Data were analyzed using 2-way ANOVA and Sidak's post-hoc  
629 test. Bar graphs (scatter plot) show mean ± SEM. Bar graphs show individual datapoints and  
630 mean ± SEM. AU = arbitrary unit.

631

632



633  
634

635 **Figure 4: Schematic showing pyruvate management in human and mouse islets. A)** In  
636 the current view (top) of  $\beta$  cell metabolism, glycolytically-derived pyruvate enters the TCA  
637 through the actions of pyruvate dehydrogenase (PDH) and pyruvate carboxylase (PC). The  
638 PEP cycle and extra-mitochondrial ADP makes a disproportionate contribution to  $K_{ATP}$  channel  
639 regulation and the triggering phase of insulin secretion. Alternative fates for pyruvate (i.e.  
640 production of lactate) are suppressed. **B)** The high-resolution view of  $\beta$  cell metabolism reveals  
641 that some pyruvate is converted to lactate, before entering into the TCA predominantly through  
642 the action of pyruvate dehydrogenase, likely to maintain REDOX and  $\beta$  cell housekeeping  
643 functions.

644  
645  
646

647 **Table 1: Human islet donor characteristics.** BMI, body mass index. IFG, impaired fasting  
648 glucose.

Unique identifier	Age group (years)	Gender	BMI (Kg/m <sup>2</sup> )	Glycemia (mmol/L)* HbA1C (%)	History of diabetes**	Islet purity (%)	Islet culture duration (h)	Country of origin
<b>HP1404</b>	50-55	♂	29.4	7.8 mmol/L	No	80	18	Italy
<b>HP1406</b>	60-65	♂	26.1	N/A	No	90	96	Italy
<b>HP1408</b>	55-60	♀	19.0	N/A	No	90	18	Italy
<b>HP1416</b>	60-65	♂	31.1	N/A	No but IFG	75	20	Italy
<b>HP1419</b>	55-60	♂	22.8	7.3 mmol/L	No	90	18	Italy
<b>HP1431</b>	60-65	♀	26.9	8.0 mmol/L	No	90	18	Italy
<b>HI1117</b>	45-50	♂	24.0	5.4%	No	80	N/A	France
<b>HI1120</b>	50-55	♂	29.5	5.7%	No	90	N/A	France
<b>HI1121</b>	60-65	♂	32	5.5%	No	90	N/A	France

649